Experimental study on the optimisation of azo-dyes removal by photo-electrochemical oxidation with TiO_2 nanotubes

Laura Mais, Annalisa Vacca, Michele Mascia, Elisabetta Maria Usai, Stefania Tronci, Simonetta Palmas*

Dipartimento di Ingegneria Meccanica, Chimica, e dei Materiali, Università degli Studi di Cagliari, via Marengo 2, 09123 Cagliari, Italy

*simonetta.palmas@dimcm.unica.it

Abstract

An experimental investigation is here presented on the photo-electrochemical removal of Methyl Orange (MO), selected as a model of the organic dyes, contained in wastewaters. The process is carried out in an electrochemical flow reactor, in which titania nanotubular electrode is irradiated with a simulated solar light. Design of Experiments (DOE) technique is used to plan the experimental campaign and investigate on the single and combined effects of applied current, electrolyte flow rate, and initial MO concentration, on the specific reaction rate. The results of the DOE analysis, also combined with the study of the distribution of the intermediate products, confirm a reaction mechanism mediated by •OH radicals; high applied current and low reactant concentration resulted as favourable conditions to achieve high specific reaction rate of colour removal.

Keywords: Advanced oxidation; Photo-electrochemical degradation; azo-dyes; Design of Experiments, TiO_2 nanotubes

1. Introduction

Industrial wastewaters may constitute a problem for living organisms and environment, especially when they contain organic substances refractory to the common treatment methods. Among the others, organic dyes are of serious concern: of note, about 15% of dyes are discharged directly into

water bodies without any treatment (Wang et al., 2017). Moreover, the common biological processes of degradation and discoloration are ineffective on modern dyes, because of the high degree of aromatic groups in their molecules (Liu et al., 2017). The traditional physical methods such as active carbon adsorption (Zhang et al., 2018), reverse osmosis (Al-Bastaki, 2004) and coagulation (Dragan and Dinu, 2008) are costly, and in most of the cases, they provoke just a change in the phase of the dye, rather than its degradation (Geng et al., 2018) (Janus and Morawski, 2007) (Kaur and Singh, 2007).

In these cases, advanced oxidation process (AOP), based on the action of strong oxidizing agents, such as $^{\bullet}OH$ radicals, are needed to keep the pollution level under the legal limits, so allowing the discharge of the effluent in the final water body. Among the AOP, those based on the electrochemical generation of $^{\bullet}OH$, have become increasingly important. In the last decade, the cost of electricity generated from wind and solar photovoltaic has fallen (to 0.045 \$ kWh^{-1} and 0.050 \$ kWh^{-1}, respectively), and it is now competitive with fossil fuel based electricity generation technologies (0.055 \$ kWh^{-1}) (Orella et al., 2018): we may then understand the renewed increased interest of the academic and industrial world, towards the so-called “processes electrification” in which the electrical energy, is used not only in the automotive sector, but also for chemical processes. And the framework could be more favourable when, thanks to the wide progresses in the field of material science, also the accumulation/storage systems will be optimized, and problems connected to the intermittence of the sources will be overcome.

In this context, photo-electrocatalysis, the subject of the present study, represents a technique in which the electrical current is used to increase the efficiency of the action of the light over a semiconductor, at which a chemical reaction occurs. In fact, from an electrochemical point of view, the presence of light energy leads to a depolarization of the electrode, while from a photo-catalytic side, application of a bias potential allows reducing the recombination of the electron-hole couples, photo-generated at the semiconductor. These two factors could result in a synergetic effect, which

in turn results in lowering the costs of the whole process (Matarrese et al., 2019) (Mais et al., 2019 a).

In the present case, a nanotubular structured semiconductor of TiO_2, irradiated with a solar light simulator, is proposed as photo-anode for the photo-electrochemical removal of Methyl Orange (MO), an organic dye used as model substance. The photo-electrochemical degradation of organics in general, and of MO in particular, has been widely studied in literature (Garcia-Segura and Brillas, 2017) (Pacheco-Alvarez et al., 2018) (Mansouri et al., 2019) (Da Dalt et al., 2013) (Ma et al., 2017): small electrochemical cells, are generally used in which small electrodes (surface area in the order of cm^2) are adopted, irradiated by UV light, while fewer papers are reported on greater engineered flow cells (Chaiyont et al., 2013) (Martín de Vidales et al., 2016) (Moura et al., 2016) (Mais et al., 2019 b).

In this work a photo-electrochemical reactor was used, which operated in continuous mode, with electrodes of 13.5 cm^2 surface area: the fluid dynamics was studied for a possible scale-up of the system. Real irradiation conditions were simulated supplying the light by a solar light simulator. The design of experiments (DOE) technique has been used to plan the experimental campaign, that allowed investigating on the influence of the different parameters on the objective function selected. The applied electrical current has been considered, along with the electrolyte flow rate and the initial reactant concentration, among the possible parameters which may influence the colour removal process, which is one of the concerns of these kind of effluents. However, attention has been paid not only to the colour removal, generally connected with the initial attack of the molecule, but also to the fate of the intermediates originated during the degradation process. Thus, for example, in combined treatment processes, depending on the treatment stage which is possibly planned after the photo-electrochemical step, the complete degradation of the organics could not be needed. In these conditions, controlling the different parameters which affect the whole process mechanism, could become a very useful practice, to decide the final extent of degradation to be

reached, or to address the reaction towards intermediate compounds which are worth to be maximised.

2. Materials and methods

2.1 DOE model

In such systems, where a large number of factors are influent, finding the optimal combination of operative conditions which allow the best performance, could become very difficult and costly, in terms of both reagent costs for the experiments, and working time of operators.

DOE represents a useful technique to individuate the minimum number of experiments necessary to evaluate single and combined effects of the investigated parameters on the objective function.

In the present case, we assumed the specific degradation rate (k_{app}) of MO as the objective function, and we evaluated the effects on it of three parameters investigated at two variation levels: applied current (I: 0.14 – 2.5 mA), flow rate, (Q: 70 – 120 mL min^{-1}), and initial reactant concentration (C: 10 – 50 mg L^{-1}).

In order to derive reliable estimation of the relative size of the effects, coded levels of the parameters have been used: the conversion of each original variable, A_i, to the coded one, x_i, was done by the following formula:

$$x = (A - A_0)/step \quad (1)$$

where $A_0 = (A_{max} + A_{min})/2$ and $step = (A_{max} - A_{min})/2$

so that *High* and *Low* levels of *x* are represented by +1 and -1, respectively.

As indicated by the technique, the influence of the parameters on the objective function Y is measured, planning the runs in which the parameters are suitably set. For a full factorial design, in

which three parameters are considered at two levels, 8 runs ($N = 2^3$) are needed to evaluate the effects.

Table 1 summarises the combination of the different coded parameters, while the following relation is adopted to evaluate the effects of the i-th parameter

$$E_i = \bar{Y}^+ - \bar{Y}^- = (\sum Y_i^+ - \sum Y_i^-)/4 \quad (2)$$

where Y^+ and Y^- represent the mean of the values of the responses obtained from runs in which the i-th parameter was set at the highest (+1) and lowest (–1) levels, respectively.

Table 1

In order to evaluate the combined effects between two parameters ij, Eq. 2 can be still used if the related columns (i*j) in Table 1 are considered to identify the maximum and the minimum levels of the combination of parameters.

Replication of the experiments (N = 2) allowed to evaluate the standard error (SE) and the standard deviation (SD) in accordance with the following relations:

$$SD = \sqrt{\sum (X - X_m)^2/(N-1)} \quad (3)$$

$$SE = \mathrm{SD}/\sqrt{\mathrm{N}} \quad (4)$$

SE in the range of 1.4×10^{-7} to 1.6×10^{-5} s^{-1}, was evaluated in our case.

Finally, a relation between variables x_i and the response Y was modeled as:

$$Y = \beta_0 + \sum_{j=1}^{k} \beta_j x_j + \sum_{i<j} \sum \beta_{ij} x_i x_j \quad (5)$$

where the coefficients, β, are estimated from the least squares method.

2.2 Mass transfer analysis

Mass transfer coefficients (k_{mFC}) were determined from cathodic limiting current densities (i_{lim}) of the ferro/ferricyanide redox probe (FC): 1 mM $K_3Fe(CN)_6$ in 0.5 M Na_2CO_3 was used with excess of $K_4Fe(CN)_6$ (0.1 M) to ensure that the anodic reaction never became the limiting process. A ramp of potential was applied to the cell (scan rate 1 mV s^{-1}); depending on the flow rate, a wide current plateau was obtained, in the potential range from about -0.9 V to -1.5 V (data not shown), corresponding to the limiting current conditions.

The mass transfer coefficients for the different flow rates were derived by the following equation (Greef et al., 1985):

$$k_m = i_{lim}/z\,F\,C_0 \qquad (6)$$

where C_0 is the concentration of FC ions, z is the number of electrons, and F is the Faraday constant. Values of mass transfer coefficients for MO (k_{mMO}) were then calculated: since dynamic viscosity of diluted aqueous solutions is poorly influenced by the electrolyte composition, the values of k_{mMO} were evaluated from the values of k_{mFC}, and diffusivity of MO and FC (D_{MO} = 6.3 × 10^{-6} cm^2 s^{-1} and D_{FC} = 6.41 × 10^{-6} cm^2 s^{-1}) by eq. 7 (Walsh, 1995) (Polcaro et al., 2007):

$$km_{MO} = km_{FC}(D_{MO}/D_{FC})^{2/3} \qquad (7)$$

k_{mMO} of 3.2 x 10^{-3} cm s^{-1} (Q = 70 mL min^{-1}) and 4.4 x 10^{-3} cm s^{-1} (Q = 120 mL min^{-1}) were obtained.

2.3 Experimental set-up

TiO_2 nanotubular structure has been obtained by anodization of Ti disks (5 cm diameter, 0.25 mm thickness, 99.7% metal basis, Aldrich), with the two-electrode cell showed in fig. 1a. The working electrode was located at the bottom of the cell with an aluminium disc to ensure the electric contact; the cathode was a grid of platinized Ti; the interelectrode gap was 1 cm; the exposed geometrical area of the anode was 13.5 cm^2.

Figure 1.

Prior to the electrochemical oxidation, Ti foils were sonicated in acetone, isopropanol and methanol, (10 minutes in each solvent); then, they were rinsed with deionized water and dried in a Nitrogen stream. The electrolytic solution used for the anodization (at room temperature) of Ti foil was composed by 0.14 M of NH_4F in deionized water (10%) and glycerol (90%). A potential ramp was imposed from open circuit voltage (OCV) to a fixed potential of 20 V with a scan rate of 100 mV s^{-1}. The applied potential was maintained at this fixed value for 4 h. A final annealing treatment was performed, in air atmosphere at 400 °C for 1 h, in order to transform the amorphous structure into a crystalline one.

The uniformity and repeatability of the nanometric structure obtained with the cell and the procedure described was already assessed by our research group (Palmas et al., 2016).

The obtained TiO_2 nanotubular samples were used as anode in the cell in fig. 1 b) for the photo-electrochemical studies. The cathode was a Pt ring in the inner surface of the cylindrical body, to avoid shadows on the working electrode; the cell was closed with a quartz window and it was set in front of the light source at 8 cm distance. The cell was inserted in a hydraulic circuit (fig. 1c) in which the electrolyte (V = 75 mL) was pumped by a peristaltic pump from the reservoir to the cell and back in a closed loop. Photo-anodes were irradiated by a 300 W xenon lamp equipped with air mass (AM) 0 and 1.5 D filters to simulate the solar irradiation.

Electrochemical measurements were recorded using a potentiostat-galvanostat (Metrhom Autolab 302N, Metrohm Switzerland), controlled by NOVA software.

Photo-electrochemical oxidation of MO was investigated by performing galvanostatic electrolyses of aqueous solutions at different operative conditions (table 1) in 0,1 M $NaClO_4$. During the runs, samples were withdrawn and analysed for the concentration of reactant by using UV-Vis spectrophotometer (Agilent Technologies Cary Series Spectrophotometer). Depending on the runs, specific analyses were also performed by HPLC (equipped with column Varian C18 with an UV detector (500 and 254 nm); the mobile phase was CH_3OH + 0.1% H_3PO_4 and 0.1% H_3PO_4 = 20:80 with a flow rate of 1 mL min^{-1}). Chromatographic peaks were identified by comparison with pure standards.

3. Results and discussion

Based on the plan indicated by DOE, 8 experimental runs were performed at the relevant operating conditions indicated in the first three columns of Table 1. Tests were repeated in duplicates. Results are resumed in Figure 2.

Figure 2

Figure 2a) shows MO removal with the supplied charge, from which indications on the yield of the process can be obtained. High removal of the reactant was achieved under all the examined conditions; at low current values the removal of MO was effective and almost complete, after 4 C of charge supplied, while a lower yield was measured at higher current.

Information on the kinetics of the process, can be derived from trend of ln (C/Co) vs time (figure 2b). A linear trend is observed under all the experimental conditions, indicating that a pseudo-first order kinetics (eq. 8) could be used to interpret the data:

$dC / dt = -k_{app} \ C$ (8)

The values of $k_{app,}$ have been valuated from the slope of each straight line at the relevant operative conditions.

Of note, although an effect of the flow rate is observable, the oxidation process is not controlled by mass transfer. The linearity of the trend $\ln(C/C_0)$ vs time indicates a mass transfer control, only if k_{app} is equal to the mass transfer rate $a\ k_{mMO}$, (being $a = A_e / V$ the ratio between geometrical area of the electrode A_e and volume V of the electrolyte): the MO decay could then be expressed by eq. 9:

$dC/dt = -a\ k_{mMO}\ C$ (9)

In the present case, the k_{app} values (see table 1) are lower than the corresponding values of ak_{mMO} at the relevant flow rates (5.80×10^{-4} s^{-1} at Q = 70 mL min^{-1} and 8.02×10^{-4} s^{-1} at 120 mL min^{-1}), confirming that the removal of MO can be considered a mixed controlled process, and not only the flow rate, but also the applied current and the initial MO concentration should be considered to correctly describe the process.

To evaluate the effects of all the variables DOE analysis was done: k_{app}, was assumed as Yi values of the objective function in Table 1, single and combined effects of each parameter were obtained with eq. 1, while the variance analysis allowed evaluating their significance within 95% of confidence level.

The analysis was carried out in two steps. The results of the first step showed that the single effects of all parameters are significant (p value < 0.05), while only the binary effects of I*Q and Q*C are. Then, the analysis has been repeated excluding the non-significant effects: the final Pareto chart and variance table are shown in figure 3.

Figure 3

Figure 4 resumes the results of the analysis. Figure 4a shows single effects of the parameters, while figure 4b) shows the so-called interaction plots which compare the binary effects. In figure 4a positive or negative slopes indicate positive or negative effects. Parallel segments in figure 4b indicate no interaction, while combined effects are evidenced when the segments are not parallel and tend to cross each other.

Finally, quantification of the different effects allowed deriving equation 10, as final model able to describe the dependence of the objective function on the three investigated parameters, (in terms of uncoded units) by the following polynomial equation:

$$k_{app}(s^{-1} \times 10^5) = 4.45 + 0.273\ I + 0.0494\ Q - 0.0614\ C + 0.01858\ I \times Q - 0.001119\ Q \times C \quad (10)$$

The values of the coded coefficients, along with their statistics are reported in fig. 4,

Equation 10 was in turn used to derive the contour plots, also reported in figure 4 (c, d, e).

Figure 4

Data in figure 4 confirm that: i) the initial MO concentration has the highest effect, which is negative (the higher the initial concentration the slower the MO removal process), while the applied current and the flow rate have a positive effect, so that higher values of k_{app} are obtained at higher current and higher flow rate.

Interaction plots and contour plots in figure 4 help to understand that the effects of current and flow rate are interconnected. So, the extent of the gain in k_{app}, obtained by increasing I, is greater when the process is performed at high Q, rather than when a low Q is adopted. Analogously, combined effect occurs between Q and C: the effect of the flow rate on k_{app} is about null at high concentration, but it becomes positive when low concentration is used. The almost parallel segments related to I*C interaction in figures 4b and 4e confirm the negligible combined effect between current and concentration, so that this effect does not appear in the model.

Finally, the model has been verified by means of a last experiment carried out at I =1.5 mA, Q = 100 mL min^{-1}, C_0 = 20 mg L^{-1}. A value of k_{app} = 8.67 x 10^{-5} s^{-1} was evaluated from the *ln* C/C_0 trend with time, which differs by 3% from that estimated by the model (eq. 10) in the same conditions.

As the reaction mechanism is concerned, it is well know that oxidation of MO in photoelectrochemical processes is mediated by hydroxyl radicals produced from water oxidation (Nosaka et al., 2003). These very reactive species can oxidize MO up to mineralization, through: i) breakdown of the azo bond, ii) opening of the aromatic ring and iii) formation of small molecules such as oxalic and maleic acids (Nie et al., 2017).

The positive effect of the applied current showed by DOE analysis agrees with a process controlled by •OH radicals: the higher the applied current, the higher the production of •OH radicals. The light absorption of dye and the adsorption of reactant could explain the negative effect of the initial reactant concentration on the color removal rate, since with high concentration of reactant, the molecules of dye could be adsorbed to the surface in such a high extent, that the active sites for the generation of •OH could be shielded (Mais et al., 2019 b).

In order to study the distribution of the intermediates, samples were analyzed by UV-vis spectrophotometry. Depending on the runs, specific analyses were also performed by HPLC: oxalic acid, maleic acid and hydroquinone were identified as the main intermediates. The trends with time of the UV-vis spectra of the samples collected during the runs under different operative conditions are compared in figure 5. The spectra are grouped in two columns, according with the two levels of initial MO concentration, being it the most influent parameter in the previous analysis.

The two peaks at 466 nm and 269 nm were attributed to MO, respectively to the chromophore N=N group and the benzene ring, while the peaks at wavelengths lower than 245 nm were referred to aromatic compounds which originate from the cleavage of the azo bond, and to aliphatic

compounds originated from opening of the benzene ring (peak at 200-220 nm) (Joseph and Mathew, 2014) (Shen et al., 2015).

Figure 5

From the comparison between the different spectra, it can be observed that the previously investigated parameters have a certain influence on the decrease in the peaks related to both MO and intermediates.

We can observe for example, the binary effect I*C. The effect of the current is different, depending on the couple of runs performed at high (runs 5-6) or low (runs 1-2) levels of concentration. With high initial concentration, the accumulation of aliphatic intermediates is greater at high (run 6) than at low (run 5) applied current. An opposite effect is revealed from the comparison between runs at low concentration, that shows a greater accumulation of aliphatic at the lowest current (run 1) rather than at highest current (run 2).

4. Conclusions

In this work we presented a study on the photo-electrochemical treatment of an aqueous solution containing methyl orange, selected to represent the class of organic dyes, often present in wastewaters.

An experimental campaign has been planned by the DOE technique to monitor the color removal process, connected to the initial breakdown of the azo bond in the chromophore group. The opening of the aromatic ring and the possible accumulation of intermediate products have also been followed during the runs.

The results demonstrated that, under the experimental conditions investigated the color removal occurred under mixed control, where initial concentration of the reactant and applied current were the most influent parameters.

A positive effect of the applied current resulted from DOE analyses, which agrees with a process mediated by $^{\bullet}OH$ radicals, while a possible effect of light absorption of the dye, along with adsorption of the dye molecules at the electrode surface, could justify the high negative effect of initial reactant concentration.

Under the examined conditions, the three operating parameters I, Q and C, also affect the extent of the degradation and the related distribution of the reaction products. Moreover, a qualitative comparison of the UV-Vis spectra indicated different effects of the parameters on k_{app} and accumulation of intermediates. Thus, for example the binary effect I*C, which resulted not significant on k_{app}, seems to be effective on the accumulation of intermediates.

Based on the presented results, we could conclude that, when the interest of the treatment is just the color removal of the wastewater, high rate of color removal may be obtained at high current and low initial concentrations, the highest yield being achieved operating at low current and low concentration. Under the worst conditions of our process, a cost of 0.3 Euro m^{-3} can be estimated for the treatment of wastewater with an average MO concentration of 50 mg L^{-1}, in agreement with the literature (Bilińska et al., 2016).

Acknowledments: This activity is supported by P.O.R. SARDEGNA F.S.E. 2014-2020 - Asse III "Istruzione e Formazione, Obiettivo Tematico: 10, Obiettivo Specifico: 10.5, Azione dell'accordo di Partenariato:10.5.12 "Avviso di chiamata per il finanziamento di Progetti di ricerca – Anno 2017" and by Sotacarbo S.p.A CEEP-2 Project, CUP D83C17000370002.

The authors thank Daniele Porcu for his support in the experimental work.

References

Al-Bastaki, N., 2004. Removal of methyl orange dye and Na_2SO_4 salt from synthetic waste water using reverse osmosis. Chem. Eng. Process. Process Intensif. 43, 1561–1567. https://doi.org/10.1016/j.cep.2004.03.001

Bilińska, L., Gmurek, M., Ledakowicz, S., 2016. Comparison between industrial and simulated textile wastewater treatment by AOPs – Biodegradability, toxicity and cost assessment. Chem. Eng. J. 306, 550-559. https://doi.org/10.1016/j.cej.2016.07.100

Chaiyont, R., Badoe, C., de León, C.P., Nava, J.L., Recio, F.J., Sirés, I., Herrasti, P., Walsh, F.C., 2013. Decolorization of Methyl Orange Dye at IrO_2-SnO_2-Sb_2O_5 Coated Titanium Anodes. Chem. Eng. Technol. 36, 123–129. https://doi.org/10.1002/ceat.201200231

Da Dalt, S., Alves, A.K., Bergmann, C.P., 2013. Photocatalytic degradation of methyl orange dye in water solutions in the presence of MWCNT/TiO_2 composites. Mater. Res. Bull. 48, 1845–1850. https://doi.org/10.1016/j.materresbull.2013.01.022

Dragan, E.S., Dinu, I.A., 2008. Removal of Azo dyes from aqueous solution by coagulation/flocculation with strong polycations. Res. J. Chem. Environ. 12, 5–11.

Garcia-Segura, S., Brillas, E., 2017. Journal of Photochemistry and Photobiology C : Photochemistry Reviews Applied photoelectrocatalysis on the degradation of organic pollutants in wastewaters. Journal Photochem. Photobiol. C Photochem. Rev. 31, 1–35. https://doi.org/10.1016/j.jphotochemrev.2017.01.005

Geng, H., Du, P., Zhang, Z., Yao, L., Cao, K., Li, S., Sheng, P., 2018. Architecting Bi_2S_3/graphene quantum dots/TiO_2 photoelectrodes for aqueous Cr(VI)/methyl orange removal. Mater. Lett. 214, 146–149. https://doi.org/10.1016/j.matlet.2017.11.126

Greef, R., Peat, R., Peter, L.M., Pletcher, D., Robinson, J., 1985. Instrumental methods in electrochemistry. Ellis Horwood, Chichester

Janus, M., Morawski, A.W., 2007. New method of improving photocatalytic activity of commercial Degussa P25 for azo dyes decomposition. Appl. Catal. B Environ. 75, 118–123.

https://doi.org/10.1016/j.apcatb.2007.04.003

Joseph, S., Mathew, B., 2014. Microwave Assisted Biosynthesis of Silver Nanoparticles Using the Rhizome Extract of Alpinia galanga and Evaluation of Their Catalytic and Antimicrobial Activities . J. Nanoparticles 2014, 1–9. https://doi.org/10.1155/2014/967802

Kaur, S., Singh, V., 2007. TiO_2 mediated photocatalytic degradation studies of Reactive Red 198 by UV irradiation. J. Hazard. Mater. 141, 230–236. https://doi.org/10.1016/j.jhazmat.2006.06.123

Liu, W., Hu, W., Liu, J., 2017. Study on the photoreductive decolorization of azo dyes by sulfite aqua. AIP Conf. Proc. 1794. https://doi.org/10.1063/1.4971952

Ma, Q., Wang, H., Zhang, H., Cheng, X., Xie, M., Cheng, Q., 2017. Fabrication of MnO_2/TiO_2 nano-tube arrays photoelectrode and its enhanced visible light photoelectrocatalytic performance and mechanism. Sep. Purif. Technol. 189, 193–203. https://doi.org/10.1016/j.seppur.2017.08.007

Mais, L., Mascia, M., Palmas, S., Vacca, A., 2019 a. Modelling of photo-electrocatalytic behaviour of TiO_2 nanotubes under solar light irradiation. Chem. Eng. J. https://doi.org/10.1016/j.cej.2019.123136

Mais, L., Mascia, M., Palmas, S., Vacca, A., 2019 b. Photoelectrochemical oxidation of phenol with nanostructured TiO_2-PANI electrodes under solar light irradiation. Sep. Purif. Technol. 208, 153–159. https://doi.org/10.1016/j.seppur.2018.03.074

Mansouri, M., Mozafari, N., Bayati, B., Setareshenas, N., 2019. Photo-catalytic dye degradation of methyl orange using zirconia–zeolite nanoparticles. Bull. Mater. Sci. 42, 230. https://doi.org/10.1007/s12034-019-1933-y

Martín de Vidales M.J., Mais, L., Sáez, C., Cañizares, P., Walsh, F.C., Rodrigo, M.A., Rodrigues, C.A., Ponce de León, C., 2016. Photoelectrocatalytic Oxidation of Methyl Orange on a TiO_2 Nanotubular Anode Using a Flow Cell. Chem. Eng. Technol. 39, 135–141. https://doi.org/10.1002/ceat.201500085

Matarrese, R., Mascia, M., Vacca, A., Mais, L., Usai, E., Ghidelli, M., Mascaretti, L., Bricchi, B.,

Russo, V., Casari, C., Libassi, A., Nova, I., Palmas, S., 2019. Integrated Au/TiO_2 nanostructured photoanodes for photoelectrochemical organics degradation. Catalysts 9, 340. https://doi.org/10.3390/catal9040340

Moura, D.C. De, Quiroz, M.A., Silva, D.R. Da, Salazar, R., Martínez-Huitle, C.A., 2016. Electrochemical degradation of Acid Blue 113 dye using TiO_2-nanotubes decorated with PbO_2 as anode. Environ. Nanotechnology, Monit. Manag. 5, 13-20. https://doi.org/10.1016/j.enmm.2015.11.001

Nie, C., Dong, J., Sun, P., Yan, C., Wu, H., Wang, B., 2017. An efficient strategy for full mineralization of an azo dye in wastewater: A synergistic combination of solar thermo- and electrochemistry plus photocatalysis. RSC Adv. 7, 36246–36255. https://doi.org/10.1039/c7ra05797k

Nosaka, Y., Komori, S., Yawata, K., Hirakawa, T., Nosaka, A.Y., 2003. Photocatalytic OH radical formation in TiO_2 aqueous suspension studied by several detection methods, Phys Chem Chem Phys. 20, 4731–4735. https://doi.org/10.1039/b307433a

Orella, M.J., Román-Leshkov, Y., Brushett, F.R., 2018. Emerging opportunities for electrochemical processing to enable sustainable chemical manufacturing. Curr. Opin. Chem. Eng. 20, 159–167. https://doi.org/10.1016/j.coche.2018.05.002

Pacheco-Alvarez, M.O., Rodríguez-Narváez, O.M., Wrobel, K., 2018. Improvement of the Degradation of Methyl Orange Using a TiO_2 / BDD Composite Electrode to Promote Electrochemical and Photoelectro-Oxidation Processes. Int. J. Electrochem. Sci. 13, 11549–11567. https://doi.org/10.20964/2018.12.70

Palmas, S., Castresana, A., Mais, L., Vacca, A., 2016. TiO_2–WO_3 nanostructured systems for photoelectrochemical applications. RSC Adv. 103, 101671–101682. https://doi.org/10.1039/c6ra18649a

Polcaro, A.M., Vacca, A., Mascia, M., Palmas, S., Pompei, R., Laconi, S., 2007. Characterization of a stirred tank electrochemical cell for water disinfection processes. Electrochim. Acta 52,

2595–2602. https://doi.org/10.1016/j.electacta.2006.09.015

Santos, J.L.C., Geraldes, V., Velizarov, S., Crespo, J.G., 2010. Characterization of fluid dynamics and mass-transfer in an electrochemical oxidation cell by experimental and CFD studies. Chem. Eng. J. 157, 379–392. https://doi.org/10.1016/j.cej.2009.11.021

Shen, T., Jiang, C., Wang, C., Sun, J., Wang, X., Li, X., 2015. A TiO_2 modified abiotic–biotic process for the degradation of the azo dye methyl orange. RSC Adv. 5, 58704–58712. https://doi.org/10.1039/c5ra06686g

Wang, J., Li, H., Meng, S., Zhang, L., Fu, X., Chen, S., 2017. One-pot hydrothermal synthesis of highly efficient SnO_x/Zn_2SnO_4 composite photocatalyst for the degradation of methyl orange and gaseous benzene. Appl. Catal. B Environ. 200, 19–30. https://doi.org/10.1016/j.apcatb.2016.06.070

Zhang, F., Dong, G., Wang, M., Zeng, Y., Wang, C., 2018. Efficient removal of methyl orange using Cu_2O as a dual function catalyst. Appl. Surf. Sci. 444, 559–568. https://doi.org/10.1016/j.apsusc.2018.03.087

Captions

Figure 1. Axonometric sections of the cells used in anodization (A) and in photo-electrochemical tests (B); sketch of the apparatus used for photo-electrochemical experiments (C).

Figure 2- Trend of the reactant removal as a function of the supplied charge (a); trend of the logarithm of the MO concentration, normalized with respect to its initial value, as a function of the supplied charge (b) for the 8 runs at the relevant conditions indicated in table 1.

Figure 3 – Pareto Chart and Variance table for the second step of the analysis in which the not significant effects were excluded.

Figure 4 – Graphical representation of the main effects a), interaction plots b) and contour plots c) along with the statistics of the coded effects (standard error SE of the coefficients, and variance inflation factor VIF are enclosed in the statistics).

Figure 5 – UV-vis spectra of the samples collected during the runs under different operative conditions.

Table 1 – DOE working plan, in terms of coded I, Q, C variables to be set for each experimental run. The coded parameters for the evaluation of combined effects are also reported. Last column reports the apparent reaction rates (k_{app}), assumed as objective function (Y): averaged values are calculated for the repeated runs.

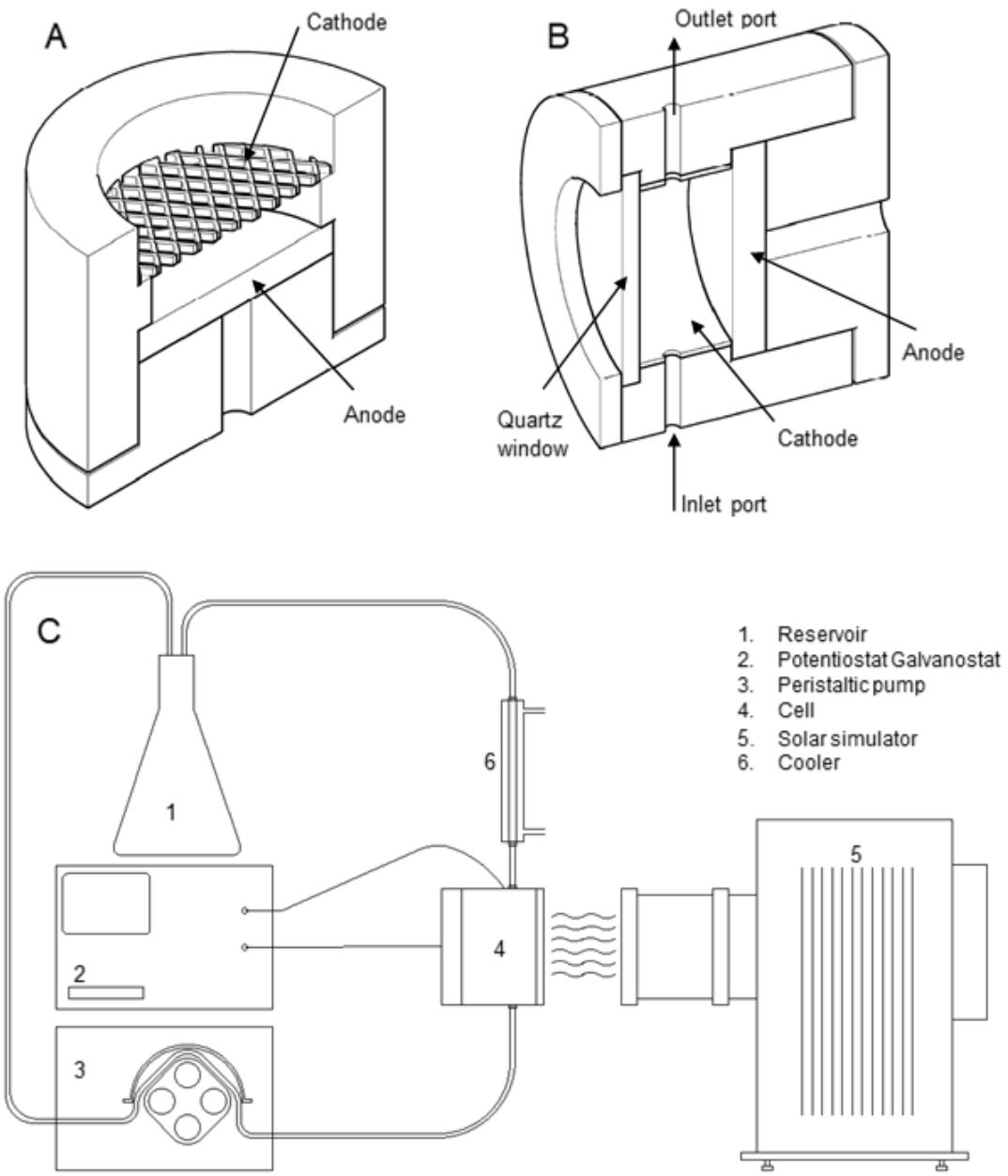
A
Cathode
Anode
B
Outlet port
Anode
Quartz window
Cathode
Inlet port
C
1. Reservoir
2. Potentiostat Galvanostat
3. Peristaltic pump
4. Cell
5. Solar simulator
6. Cooler
1
2
3
4
5
6

Fig.1

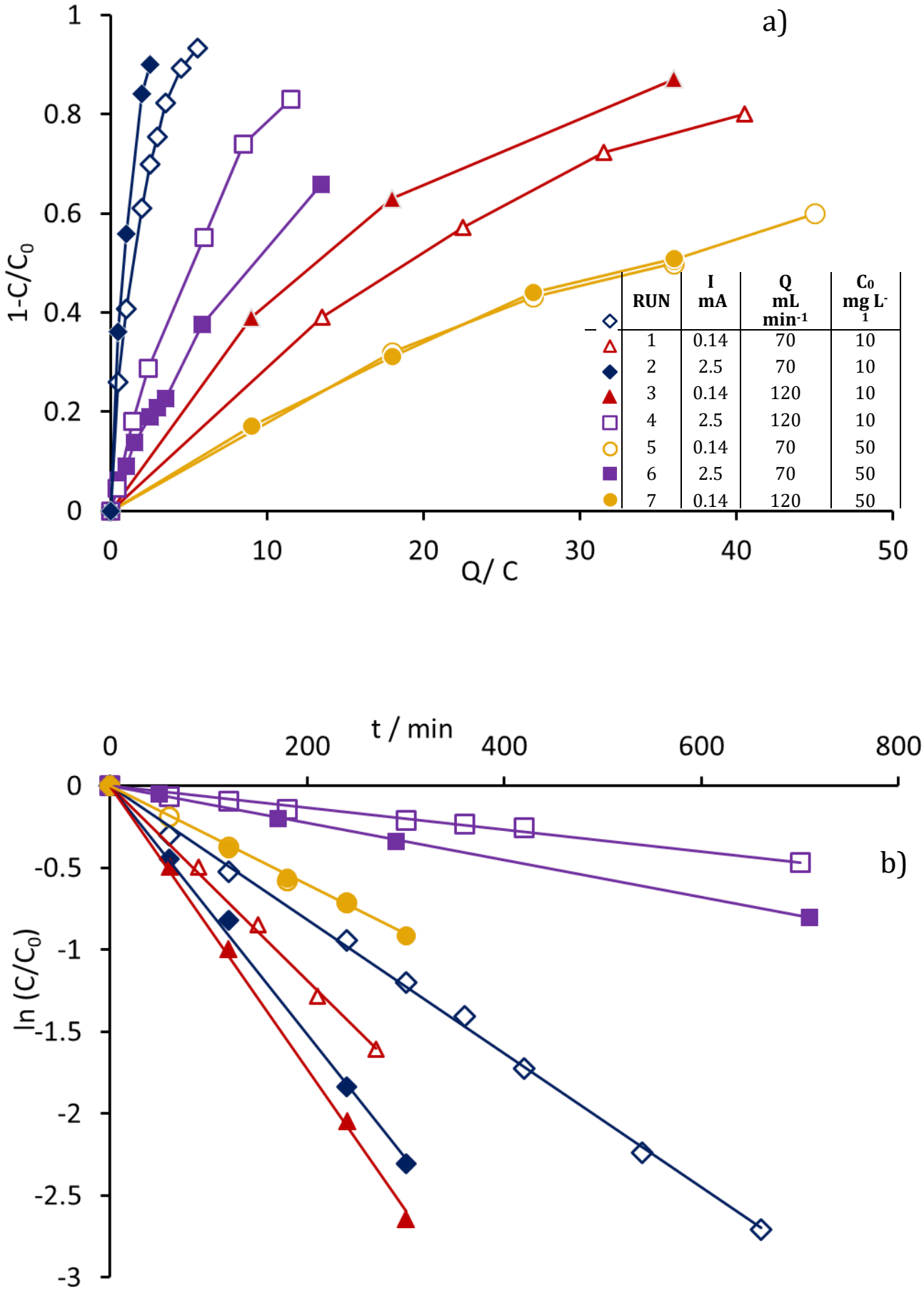
a)
1-C/C0
Q/ C
RUN
I mA
Q mL min-1
C0 mg L-1
1 0.14 70 10
2 2.5 70 10
3 0.14 120 10
4 2.5 120 10
5 0.14 70 50
6 2.5 70 50
7 0.14 120 50
b)
ln (C/C0)
t / min

Fig.2

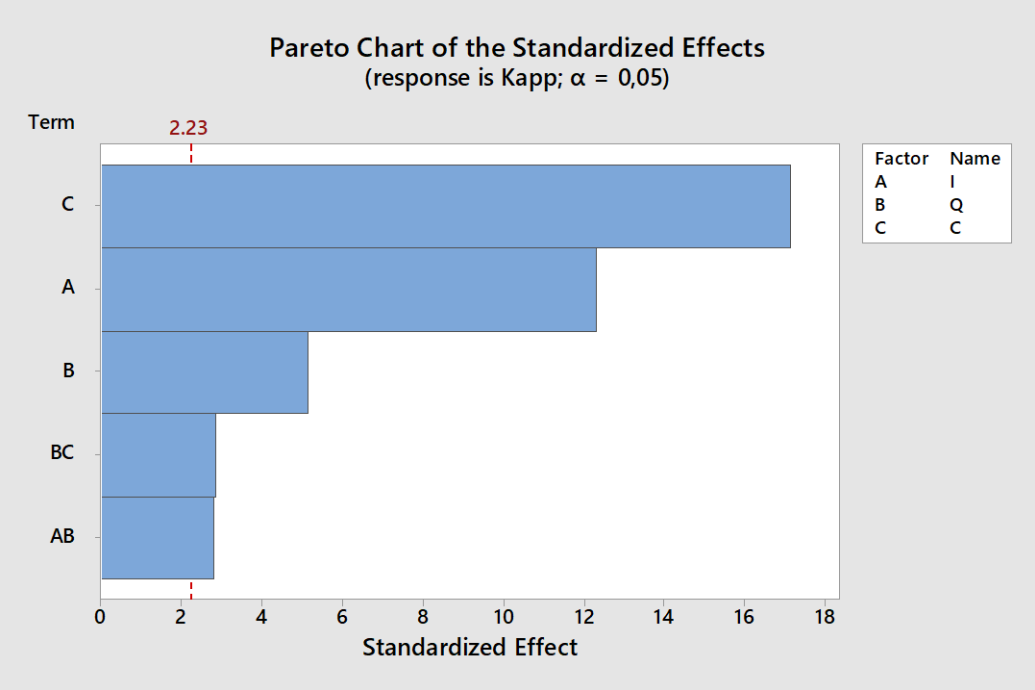

Analysis of Variance

Source	DF	Adj SS	Adj MS	F-Value	P-Value
Model	5	298.674	59.735	97.53	0.000
Linear	3	288.856	96.285	157.21	0.000
I	1	92.583	92.583	151.16	0.000
Q	1	16.257	16.257	26.54	0.000
C	1	180.016	180.016	293.91	0.000
2-Way Interactions	2	9.818	4.909	8.01	0.008
I*Q	1	4.809	4.809	7.85	0.019
Q*C	1	5.009	5.009	8.18	0.017
Error	10	6.125	0.612		
Lack-of-Fit	2	0.313	0.157	0.22	0.811
Pure Error	8	5.811	0.726		
Total	15	304.798			

Model Summary

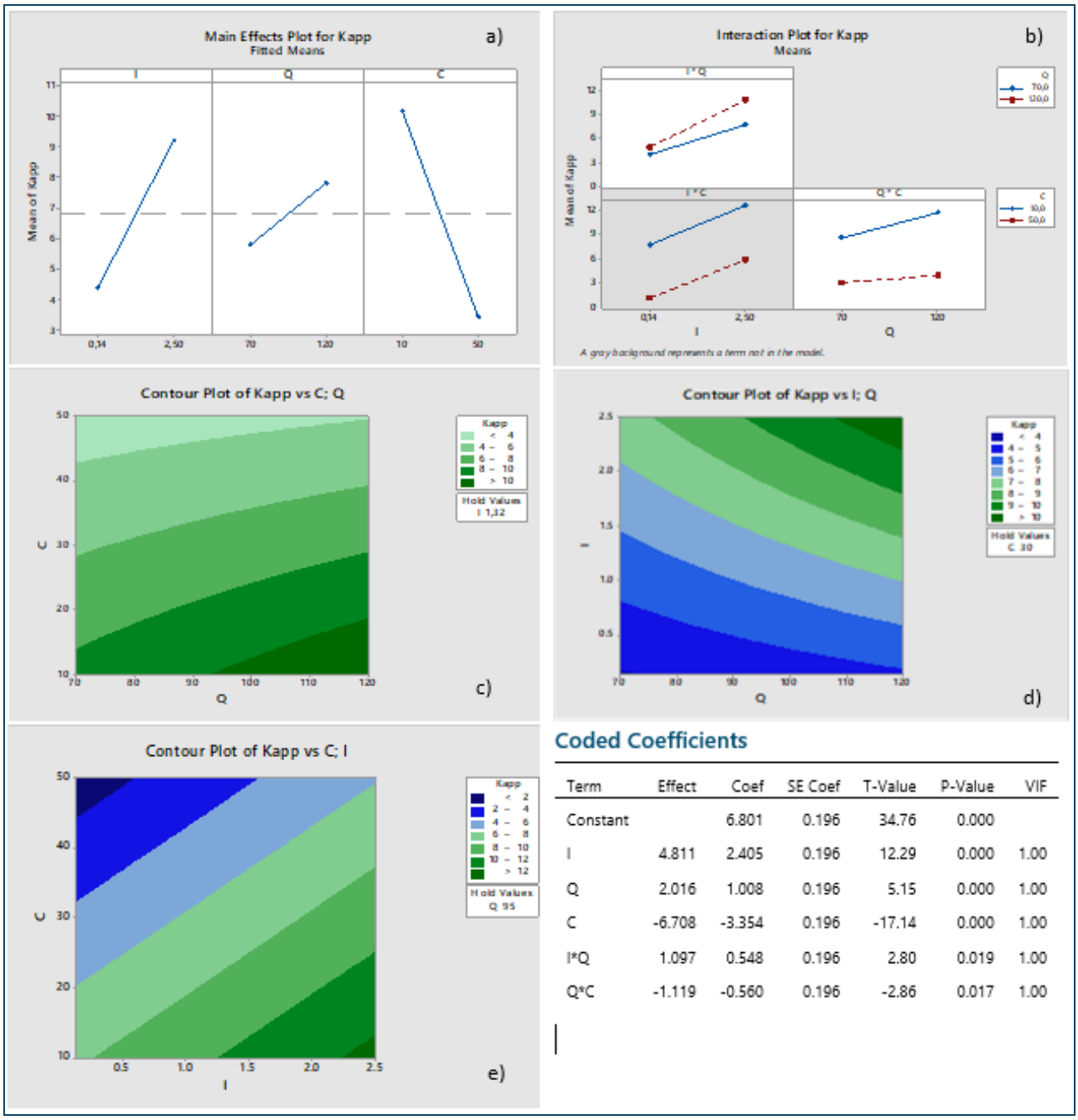

Coded Coefficients

Term	Effect	Coef	SE Coef	T-Value	P-Value	VIF
Constant		6.801	0.196	34.76	0.000	
I	4.811	2.405	0.196	12.29	0.000	1.00
Q	2.016	1.008	0.196	5.15	0.000	1.00
C	-6.708	-3.354	0.196	-17.14	0.000	1.00
I*Q	1.097	0.548	0.196	2.80	0.019	1.00
Q*C	-1.119	-0.560	0.196	-2.86	0.017	1.00

Fig. 4

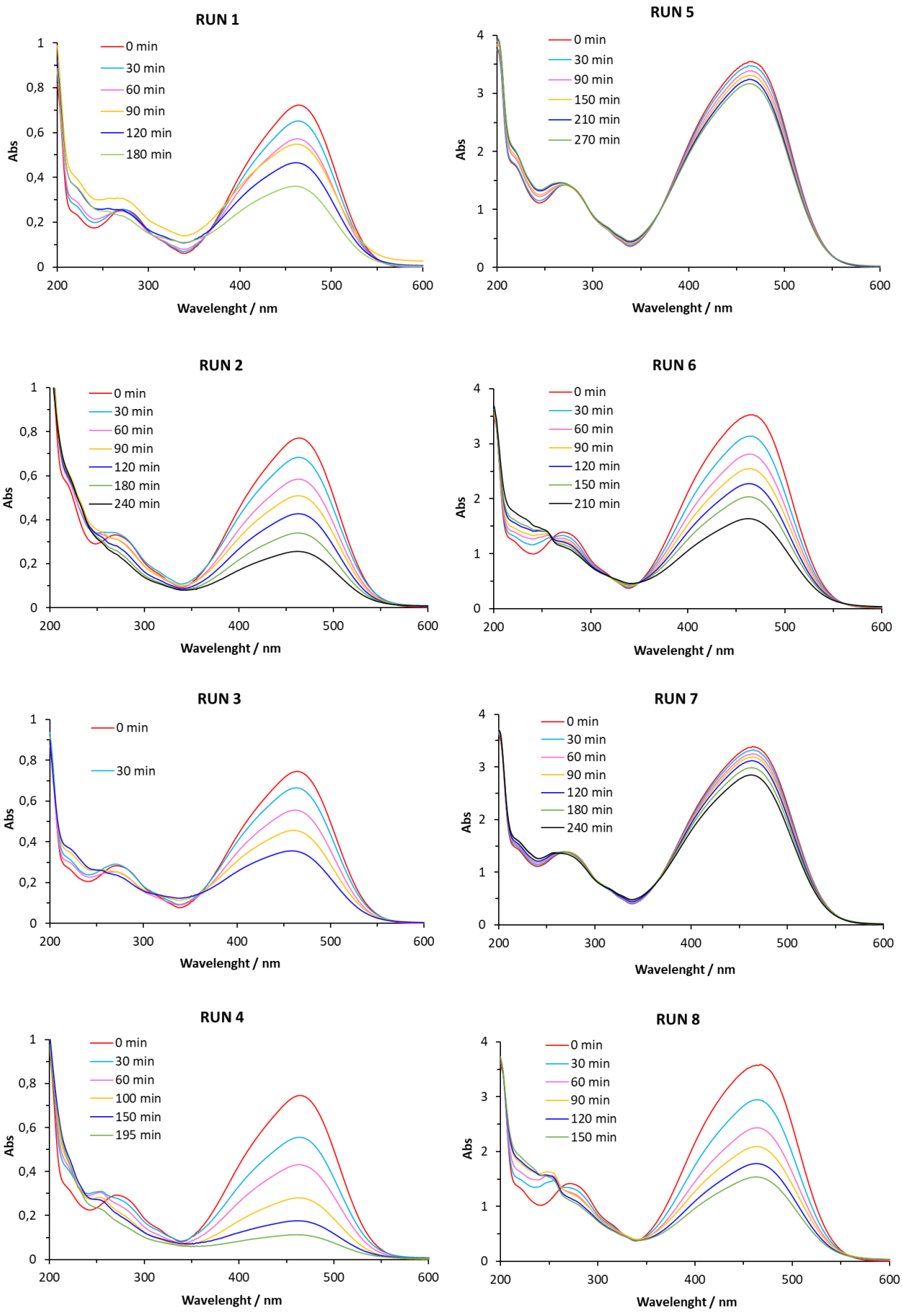
RUN 1
0 min
30 min
60 min
90 min
120 min
180 min
Abs
Wavelenght / nm
RUN 5
0 min
30 min
90 min
150 min
210 min
270 min
Abs
Wavelenght / nm
RUN 2
0 min
30 min
60 min
90 min
120 min
180 min
240 min
Abs
Wavelenght / nm
RUN 6
0 min
30 min
60 min
90 min
120 min
150 min
210 min
Abs
Wavelenght / nm
RUN 3
0 min
30 min
Abs
Wavelenght / nm
RUN 7
0 min
30 min
60 min
90 min
120 min
180 min
240 min
Abs
Wavelenght / nm
RUN 4
0 min
30 min
60 min
100 min
150 min
195 min
Abs
Wavelenght / nm
RUN 8
0 min
30 min
60 min
90 min
120 min
150 min
Abs
Wavelenght / nm

Fig. 5